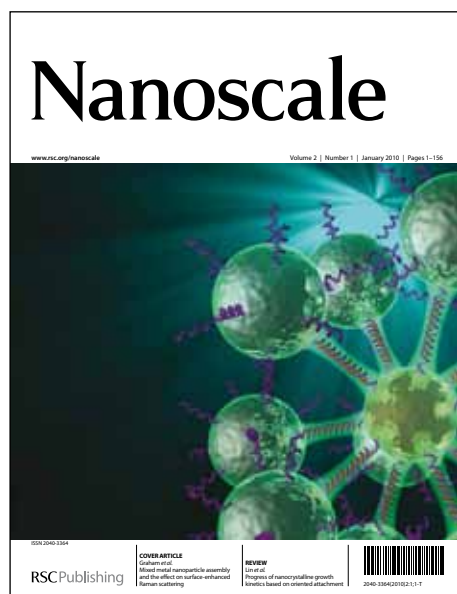


# Nanoscale

Accepted Manuscript



This is an *Accepted Manuscript*, which has been through the RSC Publishing peer review process and has been accepted for publication.

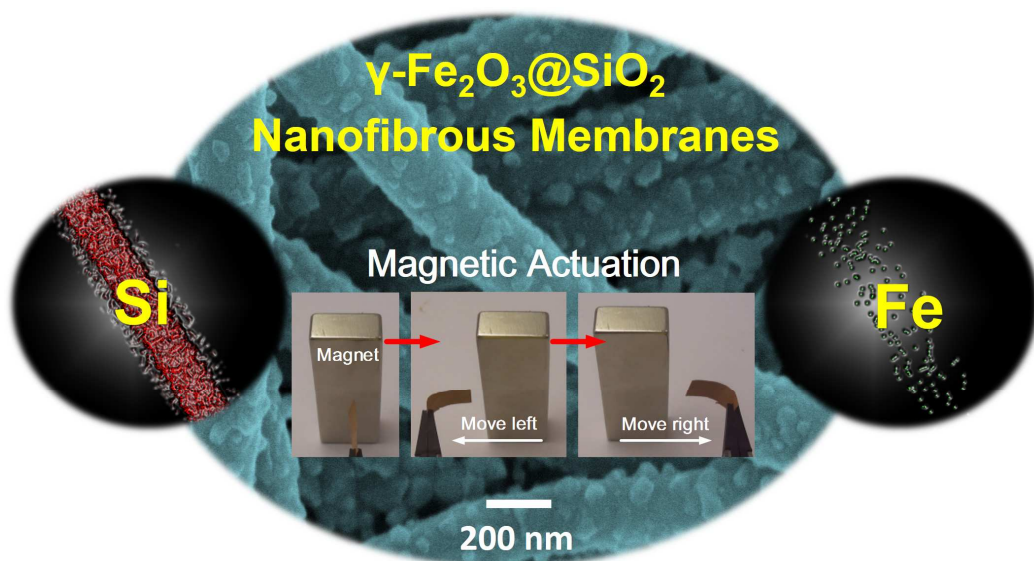
*Accepted Manuscripts* are published online shortly after acceptance, which is prior to technical editing, formatting and proof reading. This free service from RSC Publishing allows authors to make their results available to the community, in citable form, before publication of the edited article. This *Accepted Manuscript* will be replaced by the edited and formatted *Advance Article* as soon as this is available.

To cite this manuscript please use its permanent Digital Object Identifier (DOI®), which is identical for all formats of publication.

More information about *Accepted Manuscripts* can be found in the [Information for Authors](#).

Please note that technical editing may introduce minor changes to the text and/or graphics contained in the manuscript submitted by the author(s) which may alter content, and that the standard [Terms & Conditions](#) and the [ethical guidelines](#) that apply to the journal are still applicable. In no event shall the RSC be held responsible for any errors or omissions in these *Accepted Manuscript* manuscripts or any consequences arising from the use of any information contained in them.

## Graphical Abstract



Novel flexible, mesoporous, and magnetic  $\gamma\text{-Fe}_2\text{O}_3@\text{SiO}_2$  nanofibrous membranes with high  $\gamma\text{-Fe}_2\text{O}_3$  content and uniform distribution were prepared by a facile in-situ growth method.

## COMMUNICATION

## In-situ synthesis of flexible magnetic $\gamma$ - $\text{Fe}_2\text{O}_3$ @ $\text{SiO}_2$ nanofibrous membranes

Cite this: DOI: 10.1039/x0xx00000x

Yang Si,<sup>ab</sup> Xiaomin Tang,<sup>bc</sup> Jianlong Ge,<sup>bc</sup> Mohamed El-Newehy,<sup>de</sup> Salem S. Al-Deyab,<sup>d</sup> Jianyong Yu<sup>c</sup> and Bin Ding<sup>\*abc</sup>

Received 00th January 2012,  
Accepted 00th January 2012

DOI: 10.1039/x0xx00000x

www.rsc.org/

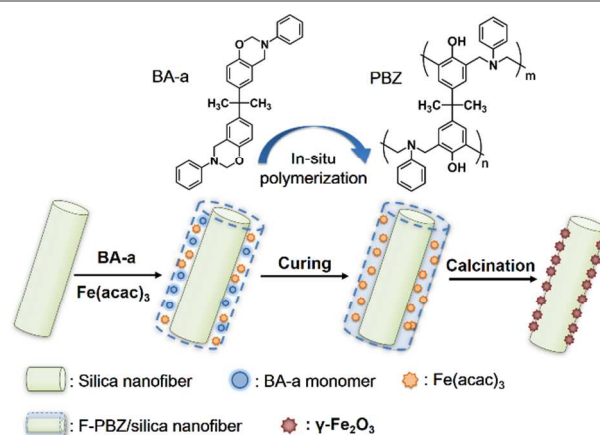
**Novel flexible, mesoporous, and magnetic  $\gamma$ - $\text{Fe}_2\text{O}_3$ @ $\text{SiO}_2$  nanofibrous membranes with high  $\gamma$ - $\text{Fe}_2\text{O}_3$  content and uniform distribution were prepared by a facile in-situ growth method, which exhibits prominent mechanical strength and magnetic responsive performance, as well as efficient adsorption for organics in water.**

Nanofiber-nanoparticle composites are attractive for use in applications requiring multifunctional characteristics, and their mechanical, optical and catalytic properties, among others, have been extensively explored.<sup>1</sup> Particularly, magnetic composite nanomaterials have attracted increasing attention encompassing such fascinating aspects as drug delivery, medical diagnosis, magnetic resonance imaging, ferrofluids and magnetic separation.<sup>2</sup> In classical methods, a minor weight fraction of surface-modified nanoparticles is simply deposited on a nanofiber matrix.<sup>3</sup> However, the nanoparticles tend to aggregate when the nanoparticle content is increased to improve material functionality, which worsens for magnetic nanoparticles due to interparticle dipolar forces.<sup>3a, 4</sup> The major challenge, therefore, is to reduce nanoparticle aggregation and control the assemblies at high concentrations, without compromising the mechanical properties of the materials.<sup>5</sup> Instead of the classic deposition of magnetic nanoparticles on a nanofiber matrix, we present an in-situ strategy using silica nanofibrous membranes (SNF) as templates for the non-agglomerated growth of  $\gamma$ - $\text{Fe}_2\text{O}_3$  nanoparticles, thereby forming ferromagnetic  $\gamma$ - $\text{Fe}_2\text{O}_3$ @ $\text{SiO}_2$  composite membranes ( $\gamma$ - $\text{Fe}_2\text{O}_3$ @SNF). Unlike solvent-swollen gels and ferrogels, our magnetic membranes are flexible, lightweight, mesoporous, and can be actuated by a small magnet. Owing to their flexibility, high porosity, and large surface area, these membranes exhibited efficient adsorption for organics in water and excellent magnetic responsive performance.

We use a bifunctional benzoxazine, namely 2,2-bis(3-phenyl-3,4-dihydro-2H-1,3-benzoxazinyl)propan (BA-a) as the novel carriers and fixatives for iron precursor, ferric acetylacetonate (( $\text{Fe}(\text{acac})_3$ )).

Scheme 1 describes the synthesis pathway. The SNF was first fabricated by the calcination of electrospun tetraethyl orthosilicate/poly(vinyl alcohol) hybrid nanofibers. Subsequently, the SNF was dipped in acetone solutions with BA-a and well dispersed  $\text{Fe}(\text{acac})_3$ , and dried in oven for 20 min. Following the in-situ polymerization of BA-a was carried out at 200°C in vacuum for 1 h, leading to the formation of the Mannich bridge cross-linked polybenzoxazine (PBZ) layer containing  $\text{Fe}(\text{acac})_3$ . Finally, the obtained membranes (PBZ/SNF) were calcined at 850°C in  $\text{N}_2$  flow to generate the reddish brown magnetic  $\gamma$ - $\text{Fe}_2\text{O}_3$ @SNF.

The representative field emission scanning electron microscopy (FE-SEM) image of SNF shown in Fig. 1a revealed a randomly oriented 3D nonwoven membranes with an average



**Scheme 1** Schematic for the in-situ strategy to the synthesis of  $\gamma$ - $\text{Fe}_2\text{O}_3$ @SNF.

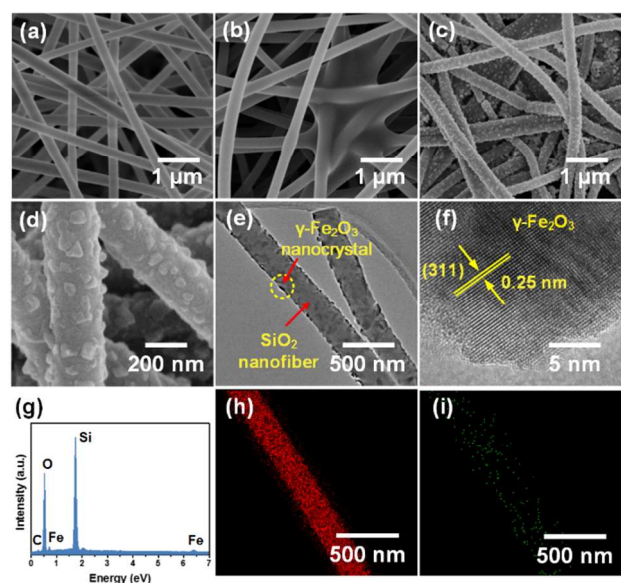


**Fig. 1** FE-SEM images of (a) SNF, (b) PBZ/SNF, and (c)  $\gamma$ -Fe<sub>2</sub>O<sub>3</sub>@SNF. (d) High magnification FE-SEM image of  $\gamma$ -Fe<sub>2</sub>O<sub>3</sub>@SNF. (e) TEM image of  $\gamma$ -Fe<sub>2</sub>O<sub>3</sub>@SNF. (f) HRTEM image showing the  $\gamma$ -Fe<sub>2</sub>O<sub>3</sub> nanocrystals in (311) orientation. (g) EDX analysis of  $\gamma$ -Fe<sub>2</sub>O<sub>3</sub>@SNF. EDX elemental mapping of (h) Si and (i) Fe, respectively, on a single fiber.

diameter of 238 nm. Upon curing at 200°C, obvious adhesion and increase in fiber diameter (264 nm) could be observed, indicating the accomplishment of in-situ polymerized BA-a on the surface of silica fibers (Fig. 1b). Moreover, transmission electron microscopy (TEM) image of PBZ/SNF (Fig. S3) showed that the PBZ layer has a uniform thickness in the range of 10–15 nm. Evidence for the formation of PBZ also came from FT-IR spectral analysis (Fig. 2a), the characteristic peaks around 1573, 1521 and 1367 cm<sup>-1</sup> were assigned to the stretching vibration of C=O, the skeletal vibration of benzene ring, and the wagging of CH<sub>2</sub>, respectively.<sup>6</sup> During the following calcination, the PBZ was gradually decomposed and carbonized, meanwhile the inner Fe(acac)<sub>3</sub> converted to magnetic  $\gamma$ -Fe<sub>2</sub>O<sub>3</sub> nanoparticles via in-situ nucleation/growth.<sup>2a,7</sup> Micrographs of  $\gamma$ -Fe<sub>2</sub>O<sub>3</sub>@SNF samples showed that the  $\gamma$ -Fe<sub>2</sub>O<sub>3</sub> nanoparticles were well located on the fiber surface without any aggregation (Fig. 1c and d), and had the sizes range from 30–70 nm (Fig. S4). A simple model of the mechanism for the non-agglomerated formation of nanoparticles on the fiber surface is presented in the Supplementary Information.

The TEM image presented in Fig. 1e showed an interesting feature that the  $\gamma$ -Fe<sub>2</sub>O<sub>3</sub> nanoparticles were partially inlaid on the silica fiber surface, which could significantly enhance the adhesion with fibers. Careful examination of corresponding HRTEM image (Fig. 1f) reveals the well-resolved lattice fringes with an interplane distance of 0.25 nm coming from the (311) plane of  $\gamma$ -Fe<sub>2</sub>O<sub>3</sub>.<sup>8</sup> Based on the semi-quantitative estimation of energy-dispersive X-ray spectroscopy (EDX), the Si, Fe, and C elements with the contents of 25.88%, 5.71%, and 1.12%, respectively, were identified in the sample (Fig. 1g), indicating the high content of magnetic  $\gamma$ -Fe<sub>2</sub>O<sub>3</sub> nanoparticles (~15 wt%)

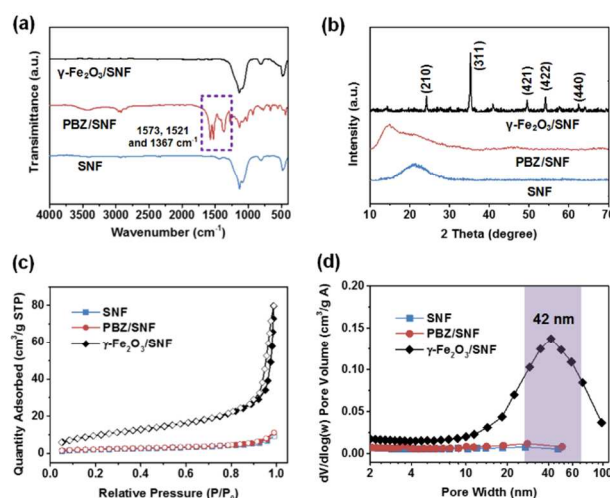


**Fig. 2** (a) FT-IR spectra of SNF, PBZ/SNF and  $\gamma$ -Fe<sub>2</sub>O<sub>3</sub>@SNF. (b) XRD patterns of SNF, PBZ/SNF and  $\gamma$ -Fe<sub>2</sub>O<sub>3</sub>@SNF. (c) N<sub>2</sub> adsorption-desorption isotherms and (d) Pore distribution analysis of relevant SNF, PBZ/SNF and  $\gamma$ -Fe<sub>2</sub>O<sub>3</sub>@SNF.

were presence in membranes.<sup>9</sup> The distribution of  $\gamma$ -Fe<sub>2</sub>O<sub>3</sub> was further verified by EDX mapping: Fe elements were shown to be uniformly distributed on the silica fibers, along with the Si elements (Fig. 1h and i). X-ray diffraction (XRD) analysis (Fig. 2b) revealed that the relevant peaks at 2 $\theta$  values of 23.9° (210), 35.3° (311), 49.6° (421), 54.1° (422), 62.5° (440) are consistent with the standard XRD data for the  $\gamma$ -Fe<sub>2</sub>O<sub>3</sub> phase (JPPDS no. 39-1346).<sup>2b, 10</sup> The crystallite sizes of  $\gamma$ -Fe<sub>2</sub>O<sub>3</sub> nanoparticles determined by Scherrer equation were in the range from 30 to 50 nm, which was in agreement with the above FE-SEM observation.

The introduction of  $\gamma$ -Fe<sub>2</sub>O<sub>3</sub> nanoparticles created the pristine silica membranes with hierarchical rough structure, thus significantly increasing the porosity and effective surface area. The relevant N<sub>2</sub> adsorption-desorption isotherms curves displayed in Fig. 2c exhibited the isotherm of type IV with a series of typical adsorption behaviors including monolayer adsorption, multilayer adsorption and capillary condensation, revealing characteristics of mesopores within the as-prepared membranes.<sup>3b</sup> The narrow H1 hysteresis loop at the region of P/P<sub>0</sub>>0.9 revealed that the mesopores are open, thus, there is no significant interruption between the capillary evaporation and condensation for N<sub>2</sub>.<sup>11</sup> Significantly, the surface area of SNF, PBZ/SNF and  $\gamma$ -Fe<sub>2</sub>O<sub>3</sub>@SNF were 7.23, 6.91 and 51.47 m<sup>2</sup> g<sup>-1</sup>, respectively, indicating the major contributing role of  $\gamma$ -Fe<sub>2</sub>O<sub>3</sub> nanoparticles on the deciding of surface area. Moreover, quantitative pore size distribution (PSD) analysis was achieved by employing the Barrett-Joyner-Halenda (BJH) method (Fig. 2d). The  $\gamma$ -Fe<sub>2</sub>O<sub>3</sub>@SNF exhibited a typically polydisperse porous structure and a primary PSD in the range of 20–60 nm, and a well-developed peaks centered at 42 nm could be observed, which matched well with the size of  $\gamma$ -Fe<sub>2</sub>O<sub>3</sub> nanoparticles. The high surface area and mesoporosity indicated that somewhat improved adsorption performances should be expected.

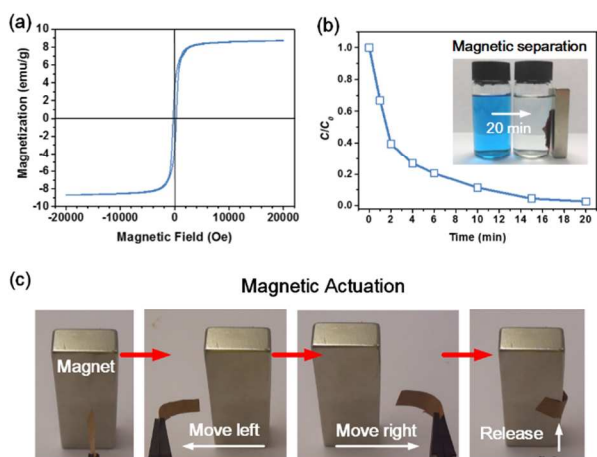


**Fig. 3** (a) Magnetic hysteresis loops of  $\gamma\text{-Fe}_2\text{O}_3\text{@SNF}$  measured at 300 K. (b) The  $C/C_0$  versus time plots for adsorption of dye solution, the inset shows the magnetic responsive of  $\gamma\text{-Fe}_2\text{O}_3\text{@SNF}$  after adsorption of MB for 20 min. (c) A piece of  $\gamma\text{-Fe}_2\text{O}_3\text{@SNF}$  membrane is held using tweezers upon a magnet (first panel), then the membrane bended towards the magnet when the tweezers move left or right (second and third panel), and it immediately flew to the magnet after being released (last panel).

The  $M$ - $H$  curve displayed in Fig. 3a showed a nonlinear and reversible behavior with a very weak magnetic hysteresis loop. This was related to the fine crystallite sizes of the inlayed  $\gamma\text{-Fe}_2\text{O}_3$  nanoparticles which were in the nanometer range, as demonstrated by the FE-SEM observations. And we believe that further decreasing the size of  $\gamma\text{-Fe}_2\text{O}_3$  by carefully changing the fabrication conditions could yield superparamagnetic membranes.<sup>28, 7</sup> Moreover, the as-prepared  $\gamma\text{-Fe}_2\text{O}_3\text{@SNF}$  exhibited a robust saturation magnetization ( $M_s$ ) of  $8.71 \text{ emu g}^{-1}$ . Taken into the consideration of the relative amount of  $\gamma\text{-Fe}_2\text{O}_3$  nanoparticles in samples ( $\sim 15 \text{ wt\%}$ ), an promising equivalent  $M_s$  of  $58.07 \text{ emu g}^{-1}$  could be analogized to the synthesized  $\gamma\text{-Fe}_2\text{O}_3$  nanoparticles.

The striking flexibility of  $\gamma\text{-Fe}_2\text{O}_3\text{@SNF}$  membranes was shown in Fig. S5, repeated bending through  $180^\circ$  causes no apparent damage (see also Movie S1). This observation is unexpected, because inorganic nanofibrous membranes are typically brittle.<sup>4, 22</sup> Fig. S6 indicated the  $\gamma\text{-Fe}_2\text{O}_3\text{@SNF}$  membranes had robust tensile strength of 1244 KPa, which was higher than that of the commercial polymer nonwoven mats. In comparison, although some inorganic magnetic nanofibers have been constructed, but their brittleness renders them impractical for most applications.<sup>7</sup> The present flexibility can be explained by the amorphous state and highly entanglement of silica nanofiber, which have high aspect ratio of larger than  $10^3$ .<sup>22</sup> Fig. 3c showed that a small iron-neodymium-boron magnet could provide reversible and large deformation of the  $\gamma\text{-Fe}_2\text{O}_3\text{@SNF}$  membranes (see also Movie S2). Previously, magnetic nanoparticle-containing solvents swollen ferrogels and hydrogels have been shown to be responsive materials and actuators, however, drying of such gels typically results in brittle materials.<sup>19, 7</sup> Our findings suggest that these dry flexible membrane actuators may be used in conditions similar to electronic devices.

As expected, the  $\gamma\text{-Fe}_2\text{O}_3\text{@SNF}$  which combined the robust porous structure and magnetic performance, demonstrated efficient adsorption for organics and fast magnetic separation property. We tested the adsorption performance for typical organic pollutant of

methylene blue (MB,  $1 \times 10^{-5} \text{ M}$ ). Fig. 3b indicated that adsorption capacity of MB was 89% for 10 min, and could achieve completely adsorption of MB for 20 min. Significantly, the  $\gamma\text{-Fe}_2\text{O}_3\text{@SNF}$  after adsorption could be separated facilely by an external magnet without tedious separation process, which is of great importance for real applications.

In summary, we have demonstrated a facile in-situ strategy to constructing magnetic  $\gamma\text{-Fe}_2\text{O}_3\text{@SiO}_2$  nanofibrous membranes with robust flexibility and porosity. The introduction of novel BA-a carrier enable the non-agglomerated growth of  $\gamma\text{-Fe}_2\text{O}_3$  nanoparticles inlayed on silica nanofiber surface, and achieving the uniform distribution and high loading content. Quantitatively porous structure analysis has indicated the major contribution of  $\gamma\text{-Fe}_2\text{O}_3$  nanoparticles on enhancing the surface area, and the majority of mesoporosity with a centered PSD at 42 nm was also confirmed. Moreover, the  $\gamma\text{-Fe}_2\text{O}_3\text{@SNF}$  exhibited prominent mechanical strength and magnetic responsive performance, as well as efficient adsorption for organics in water, which make them a good candidate to be useful in microfluidics devices and electronic actuators. This work also provided a versatile strategy for further design and development of functional nanofiber-nanoparticle composites towards various applications.

This work is supported by the National Natural Science Foundation of China (No. 51322304 and U1232116), the Program for New Century Talents of the University in China, and the Fundamental Research Funds for the Central Universities.

## Notes and references

- <sup>a</sup> State Key Laboratory for Modification of Chemical Fibers and Polymer Materials, College of Materials Science and Engineering, Donghua University, Shanghai 201620, China. E-mail: binding@dhu.edu.cn.
- <sup>b</sup> College of Textiles, Donghua University, Shanghai 201620, China.
- <sup>c</sup> Nanomaterials Research Center, Modern Textile Institute, Donghua University, Shanghai 200051, China.
- <sup>d</sup> Department of Chemistry, College of Science, King Saud University, Riyadh 11451, Saudi Arabia.
- <sup>e</sup> Department of Chemistry, Faculty of Science, Tanta University, Tanta 31527, Egypt.

Electronic Supplementary Information (ESI) available: [Detailed synthesis and structural confirmation of BA-a, TEM and flexibility results, Movie S1 and Movie S2]. See DOI: 10.1039/c000000x/

- (a) R. T. Olsson, M. A. S. Azizi Samir, G. Salazar-Alvarez, L. Belova, V. Ström, L. A. Berglund, O. Ikkala, J. Nogués and U. W. Gedde, *Nat. Nanotechnol.*, 2010, **5**, 584; (b) Z. Xu, Y. Hou and S. Sun, *J. Am. Chem. Soc.*, 2007, **129**, 8698; (c) X. Wang, B. Ding, G. Sun, M. Wang and J. Yu, *Prog. Mater. Sci.*, 2013, **58**, 1173.
- (a) Y. Si, T. Ren, B. Ding, J. Yu and G. Sun, *J. Mater. Chem.*, 2012, **22**, 4619; (b) B. Li, H. Cao, J. Shao and M. Qu, *Chem. Commun.*, 2011, **47**, 10374; (c) X. Yu, J. Wan, Y. Shan, K. Chen and X. Han, *Chem. Mater.*, 2009, **21**, 4892.
- (a) N. A. M. Barakat, B. Kim and H. Y. Kim, *J. Phys. Chem. C*, 2009, **113**, 531; (b) Y. Si, T. Ren, Y. Li, B. Ding and J. Yu, *Carbon*, 2012, **50**, 5176.
- P. Joshi, L. Zhang, D. Davoux, Z. Zhu, D. Galipeau, H. Fong and Q. Qiao, *Energy Environ.*, 2010, **3**, 1507.

## COMMUNICATION

5. (a) R. Cano, M. Yus and D. J. Ramón, *Chem. Commun.*, 2012, **48**, 7628; (b) Y. Li, W. Xiao, K. Xiao, L. Berti, J. Luo, H. P. Tseng, G. Fung and K. S. Lam, *Angew. Chem. Int. Ed.*, 2012, **51**, 2864; (c) D. Faivre, *Nat. Nanotechnol.*, 2010, **5**, 562.
6. N. N. Ghosh, B. Kiskan and Y. Yagci, *Prog. Polym. Sci.*, 2007, **32**, 1344.
7. S. Laurent, D. Forge, M. Port, A. Roch, C. Robic, L. V. Elst and R. N. Muller, *Chem. Rev.*, 2008, **108**, 2064.
8. T. Ren, Y. Si, J. Yang, B. Ding, X. Yang, F. Hong and J. Yu, *J. Mater. Chem.*, 2012, **22**, 15919.
9. X. Wang, N. G. Akhmedov, Y. Duan, D. Luebke and B. Li, *J. Mater. Chem. A*, 2013, **1**, 2978.
10. F. Jiao, J. C. Jumas, M. Womes, A. V. Chadwick, A. Harrison and P. G. Bruce, *J. Am. Chem. Soc.*, 2006, **128**, 12905.
11. R. Liang, H. Cao and D. Qian, *Chem. Commun.*, 2011, **47**, 10305.
12. M. Guo, B. Ding, X. Li, X. Wang, J. Yu and M. Wang, *J. Phys. Chem. C*, 2009, **114**, 916.